Wind and Structures, *Vol. 19, No. 6 (2014) 687-708*
DOI: http://dx.doi.org/10.12989/was.2014.19.6.687

Computational modeling of the atmospheric boundary layer using various two-equation turbulence models

Franjo Juretić and Hrvoje Kozmar*

Faculty of Mechanical Engineering and Naval Architecture, University of Zagreb, Ivana Lučića 5, 10000 Zagreb, Croatia

(Received March 21, 2014, Revised September 5, 2014, Accepted November 10, 2014)

Abstract. The performance of the k-ε and k-ω two-equation turbulence models was investigated in computational simulations of the neutrally stratified atmospheric boundary layer developing above various terrain types. This was achieved by using a proposed methodology that mimics the experimental setup in the boundary layer wind tunnel and accounts for a decrease in turbulence parameters with height, as observed in the atmosphere. An important feature of this approach is pressure regulation along the computational domain that is additionally supported by the nearly constant turbulent kinetic energy to Reynolds shear stress ratio at all heights. In addition to the mean velocity and turbulent kinetic energy commonly simulated in previous relevant studies, this approach focuses on the appropriate prediction of Reynolds shear stress as well. The computational results agree very well with experimental results. In particular, the difference between the calculated and measured mean velocity, turbulent kinetic energy and Reynolds shear stress profiles is less than ±10% in most parts of the computational domain.

Keywords: neutrally stratified atmospheric boundary layer; atmospheric turbulence; computational modeling; steady Reynolds-Averaged-Navier-Stokes (RANS) equations; two-equation turbulence models; computational wind tunnel

1. Introduction

While the turbulent Reynolds shear stress is considered to be one of the key factors influencing local wind environment with likely effects on structures, it has not been a focus of previous computational simulations of the ABL and turbulence using RANS turbulence models. In addition, a majority of studies previously performed assumes a uniform profile of turbulence parameters with increasing height, even though that is not the case in the atmosphere. These issues indicate that further work is needed with respect to a proper modeling of the wind characteristics for engineering purposes.

Computational simulations of the atmospheric boundary layer (ABL) flow have been commonly carried out using the steady RANS codes available in standard commercial CFD software (O'Sullivan *et al*. 2011), as e.g., FLUENT, OpenFOAM, STAR CD, CFX and others. This standard approach usually includes turbulence closures, grain of sand rough wall-function

*Corresponding author, Associate Professor, E-mail: hrvoje.kozmar@fsb.hr

http://www.techno-press.org/?journal=was&subpage=8 ISSN: 1226-6116 (Print), 1598-6225 (Online)

models and neutrally stable atmospheric conditions. At the moment, the common problems in this approach still seem to be longitudinal flow homogeneity, proper simulation of atmospheric turbulence and wall-function treatment. Therefore, Hargreaves and Wright (2007) argue that horizontal inhomogeneity of the computationally simulated ABL flow is due to the wall functions inconsistent with the inflow boundary profiles. Riddle *et al.* (2004) indicate the errors can be reduced by using a second order turbulence closure model. Yang *et al.* (2009), Hu *et al*. (2013) develop new, more general and more consistent inflow profiles, Zhang *et al.* (2013) propose a modified wall function, Revuz *et al*. (2012) investigate the domain size necessary when modeling wind environment around buildings. Blocken *et al*. (2007a) suggest alternative measures to reduce erroneous streamwise gradients, indicate that sensitivity tests in an empty computational domain are of critical importance. Therefore, they advise to investigate the incident flow profiles at the building position, obtained in the empty domain, because those profiles (not the profiles at the inlet of the computational domain) characterize the real flow to which the building models are subjected. In addition, Blocken *et al*. (2007b) indicate that ''modified-for-roughness'' wall functions currently implemented in many commercial CFD codes can be unsuitable for simulation of the ABL flow. The importance of the boundary conditions at the top of the domain has been highlighted by several groups, e.g., Richards and Hoxey (1993), Blocken *et al*. (2007a), Franke *et al*. (2007), Hargreaves and Wright (2007), Yang *et al*. (2009). Richards and Hoxey (1993) assume a constant profile of turbulent kinetic energy with increasing height throughout the atmospheric surface layer. Gorlé *et al*. (2009) developed a horizontally homogeneous turbulent kinetic energy profile varying with height by modifying two constants in the standard k–ε turbulence model. Parente *et al*. (2011a, b) added a source term to the transport equation of turbulent kinetic energy and dissipation to ensure equilibrium between production and dissipation, and suggested a novel rough wall function formulation.

In this study, a computational methodology using four different turbulence models has been developed in order to correctly reproduce the ABL flow above rural, suburban, and urban terrains. In addition to commonly reproduced mean velocity, turbulent kinetic energy profiles, the proposed approach achieves good agreement between the calculated turbulent Reynolds shear stress and the measured profiles as well. In the computations performed, the focus was on developing conditions enabling both the Reynolds shear stress and the turbulent kinetic energy reduce with increasing height, as observed in the wind tunnel and the atmosphere. While in previous studies the focus was on adding additional terms in turbulence models or applying a desired inlet profile, the scope of the present study is on the development of the computational setup resulting in physically acceptable wind conditions at the sampling position. The present study is a continuation of the work reported in Juretić and Kozmar (2013), where this approach was investigated in computational modeling of the neutrally stratified ABL using the standard k–ε turbulence model.

2. Wind - tunnel experiments

The computational results obtained in this study are validated using the experimental simulations of the rural, suburban, and urban ABL flow reported in Kozmar (2011a), which were carried out in the boundary layer wind tunnel at the Technische Universität München (TUM), Germany. In this wind tunnel, the flow uniformity at the inlet of the test section is achieved using a honeycomb, four sets of screens and a nozzle. A zero pressure gradient along the wind-tunnel test section is obtained by adjusting the ceiling height. Velocity measurements are recorded along the

vertical line at the turntable center, which is positioned 11.3 m downwind from the nozzle. The wind-tunnel blower is driven by a 210 kW electric motor, which allows for velocity regulation from 1 m/s to 30 m/s. More technical details about this wind tunnel can be found elsewhere (Kozmar 2011b) along with details on the experimental setup (Kozmar 2008, 2012a) and the results, which indicate a well developed and uniform ABL simulation at the sampling position. The ABL simulation technique is a modification of the original Counihan (1969a, 1969b, 1973) method based on the use of quarter-elliptic, constant-wedge-angle spires and a castellated barrier wall, followed by a fetch of surface roughness elements. In particular, experiments reported in (Kozmar 2011a) were carried out using the truncated vortex generators developed for part-depth ABL wind-tunnel simulations, together with the castellated barrier wall and surface roughness elements. In addition, the performance of the truncated vortex generators was further validated in comparison with the original full-size Counihan vortex generators for urban, suburban, and rural terrains, Kozmar (2010, 2011c, 2012b), respectively, where an agreement of wind-tunnel and full-scale results was justified by using the commonly adopted empirical rules, international standards and codes, and atmospheric physics. In particular, mean velocity profiles $\overline{u}$ agree with the power law for exponents α = 0.16, 0.20, and 0.37 in the rural, suburban, and urban ABL wind-tunnel simulations, respectively. The turbulence intensity profiles I_u, I_v, and I_w in longitudinal, lateral, and vertical direction, respectively, which were used to calculate turbulent kinetic energy k, are in good agreement with ESDU 74031 (1974). Reynolds shear stress profiles exhibit a trend of constant values in the near-ground region that is similar to the Prandtl constant-flux-layer observed in the full-scale up to 100 m, Garratt (1992) and Holmes (2007). As it is an important factor in creating a computational model, the ratio of the turbulent kinetic energy to $-\overline{u'w'}$ Reynolds shear stress, nearly-constant with the average value 4.76, is displayed in Fig. 1. In this figure, y-axis is reported in meters, as it is further used for comparison against the wind-tunnel results, while it can be transformed into non-dimensional height z^+ by using the laminar kinematic viscosity $\nu = 1.51 \cdot 10^{-5} \mathrm{m}^2/\mathrm{s}$ and the respective friction velocities u_τ reported in Table 1.

Therefore, computational results for the longitudinal mean velocity $\overline{u}$, turbulent kinetic energy k, Reynolds shear stress $-\overline{u'w'}$ profiles are compared with the experimental results at the wind-tunnel scale. Details of recorded experimental values are given in Table 1.

Table 1 Reference height z_{ref}, reference velocity $\overline{u}_{\mathrm{ref}}$, power-law exponent α, and friction velocity u_τ in ABL wind-tunnel simulations

ABL simulation	z_{ref}, m	$\overline{u}_{\mathrm{ref}}$, m/s	α	u_τ, m/s
Rural	0.202	14.97	0.16	1.11
Suburban	0.202	13.48	0.20	1.10
Urban	0.202	10.14	0.37	1.43

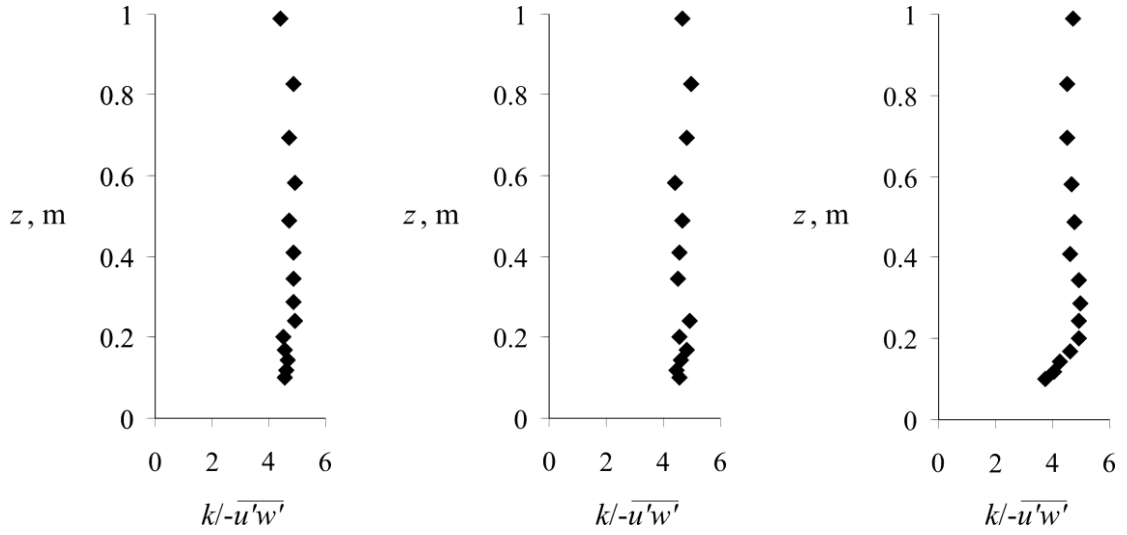

Fig. 1 Turbulent kinetic energy k to $-\overline{u'w'}$ Reynolds shear stress ratio in the (a) rural, (b) suburban, (c) urban ABL wind-tunnel simulations

3. Governing equations and applied turbulence models

Turbulent flow in the wind tunnel is predominantly 1D flow with the dominant flow velocity along the wind tunnel test section (x-direction) resulting in negligible convection terms. In addition, the Reynolds shear stresses in the wind-tunnel ABL simulation are much larger than the viscous stresses, and therefore the latter can be neglected. For this case, the full set of RANS equations simplifies to the following equation

$$-\frac{\partial}{\partial z}\overline{u'w'}(z)+\frac{\partial \bar{p}(z)}{\partial x}=0 \tag{1}$$

where $\bar{p}(z)$ represents the kinematic air pressure with the units m^2/s^2.

Four turbulence models are considered in this study: a) the standard k-ε model (Jones and Launder 1972), b) the realizable k-ε model (Shih *et al*. 1995), c) the RNG k-ε model (Yakhot and Orszag 1986), d) the standard k-ω model (Wilcox 1988). In all of these models, the Reynolds shear stress in Eq. (1) is linked with the velocity field via the Boussinesq hypothesis (1877) $-\overline{u'w'}(z)=\nu_t\,\partial\bar{u}(z)/\partial z$, and therefore the Eq. (1) can be written as follows

$$-\frac{\partial}{\partial z}\left[\nu_t(z)\frac{\partial \bar{u}(z)}{\partial z}\right]+\frac{\partial \bar{p}(z)}{\partial x}=0 \tag{2}$$

where ν_t is the turbulent viscosity and it is calculated by the turbulence model. All of the used turbulence models calculate Reynolds shear stress using the standard Boussinesq hypothesis. The conservation equations for developed boundary layers assume equilibrium between turbulence production and dissipation, and this property was used in this study as well.

3.1 The standard k-ε turbulence model

The standard *k-ε* model solves two equations, one for turbulent kinetic energy $k(z)$ and the second for turbulence dissipation $\varepsilon(z)$, Jones and Launder (1972)

$$\frac{\partial}{\partial z}\left[\frac{\nu_{\mathrm{t}}(z)}{\sigma_{k\_\mathrm{ske}}}\frac{\partial k(z)}{\partial z}\right]+P(z)-\varepsilon(z)=0 \tag{3}$$

$$\frac{\partial}{\partial z}\left[\frac{\nu_{\mathrm{t}}(z)}{\sigma_{\varepsilon\_\mathrm{ske}}}\frac{\partial \varepsilon(z)}{\partial z}\right]+C_{1\_\mathrm{ske}}\frac{P(z)\cdot\varepsilon(z)}{k(z)}-C_{2\_\mathrm{ske}}\frac{\varepsilon(z)^2}{k(z)}=0 \tag{4}$$

where the turbulent viscosity is calculated from turbulent kinetic energy $k(z)$ and turbulence dissipation $\varepsilon(z)$ using the following expression, Jones and Launder (1972)

$$\nu_{\mathrm{t}}(z)=C_{\mu\_\mathrm{ske}}\frac{k(z)^2}{\varepsilon(z)} \tag{5}$$

After introducing the Boussinesq (1877) hypothesis, the production term *P*(*z*) is modeled as follows

$$P(z)=-\overline{u'w'}(z)\frac{\partial \bar{u}(z)}{\partial z}=\nu_{\mathrm{t}}(z)\left(\frac{\partial \bar{u}(z)}{\partial z}\right)^2 \tag{6}$$

The model has five constants, i.e., C_{μ_ske}, σ_{k_ske}, $\sigma_{\varepsilon\_\mathrm{ske}}$, C_{1_ske}, and C_{2_ske}. Their standard values (Jones and Launder, 1972) are $C_{\mu\_\mathrm{ske}}=0.09$, $\sigma_{k\_\mathrm{ske}}=1$, $\sigma_{\varepsilon\_\mathrm{ske}}=1.3$, $C_{1\_\mathrm{ske}}=1.44$ and $C_{2\_\mathrm{ske}}=1.92$.

The wind-tunnel results presented in Fig. 1 indicate that the ratio between turbulent kinetic energy $k(z)$ and dominant shear stress $\overline{u'w'}(z)$ is fairly constant for all measurement points and for all terrain types, and it is used for determining the constant C_{μ_ske} according to the following expression, as given in Pope (2000)

$$\frac{1}{\sqrt{C_{\mu\_\mathrm{ske}}}}=\frac{k(z)}{-\overline{u'w'}(z)} \tag{7}$$

Eq. (7) is valid for homogeneous turbulence, when turbulence dissipation is equal to turbulence production, and it is derived by moving $\varepsilon(z)$ in Eq. (5) to the left-hand side and substituting it with the expression given in Eq. (6).

In the present study, the measurements used for validation show that the ratio between the turbulent kinetic energy and the dominant component of the shear stress is 4.76, which is larger than the value of 3.33 commonly reported for most channel flows. This ratio implies that the value C_{μ_ske}, according to Eq. (7), should be 0.044, as reported by Juretić and Kozmar (2013). In addition, the model shall satisfy the equation proposed by Richards and Hoxey (1993)

$$\sigma_{\varepsilon\_\mathrm{ske}} = \frac{\kappa^2}{(C_{2\_\mathrm{ske}} - C_{1\_\mathrm{ske}})\sqrt{C_{\mu\_\mathrm{ske}}}} \tag{8}$$

where κ is von Kármán constant with the value of 0.41. Therefore, Eq. (8) imposes constraints on $\sigma_{\varepsilon\_\mathrm{ske}}$ and the value used in this study is $\sigma_\varepsilon = 1.67$. All the calculations reported were performed with the same set of coefficients for all three boundary layer types, i.e., $C_{\mu\_\mathrm{ske}} = 0.044$, $C_{1\_\mathrm{ske}} = 1.44$, $C_{2\_\mathrm{ske}} = 1.92$, $\sigma_{k\_\mathrm{ske}} = 1$, $\sigma_{\varepsilon\_\mathrm{ske}} = 1.67$. The adopted set of coefficients is similar to the one proposed by Duynkerke (1988), i.e., $C_{\mu\_\mathrm{ske}} = 0.033$, $C_{1\_\mathrm{ske}} = 1.44$, $C_{2\_\mathrm{ske}} = 1.92$, $\sigma_{k\_\mathrm{ske}} = 1$, $\sigma_{\varepsilon\_\mathrm{ske}} = 1.67$, which is developed through the comparison of the computational modeling and atmospheric observations indicating strong effects of stability disturbances on the neutrally stratified ABL.

3.2 The realizable k-ε turbulence model

The realizable *k-ε* turbulence model also consists of two equations, i.e., one for the turbulent kinetic energy $k(z)$ as given in Eq. (3), and the turbulence dissipation $\varepsilon(z)$ as suggested by Shih *et al*. (1995)

$$\frac{\partial}{\partial z}\left[\frac{\nu_\mathrm{t}(z)}{\sigma_{\varepsilon\_\mathrm{rke}}}\frac{\partial \varepsilon(z)}{\partial z}\right] + C_{1\_\mathrm{rke}} S(z)\cdot\varepsilon(z) - C_{2\_\mathrm{rke}}\frac{\varepsilon(z)^2}{k(z)+\sqrt{\nu\,\varepsilon(z)}} = 0 \tag{9}$$

$S(z)$ is the magnitude of the strain tensor calculated using the expression $S(z) = \sqrt{2S_{ij}(z)S_{ij}(z)}$, where $S_{ij}(z) = \frac{1}{2}\left(\frac{\partial u_i}{\partial x_j} + \frac{\partial u_\mathrm{j}}{\partial x_i}\right)$, which simplifies to $S(z) = \frac{1}{2}\frac{\partial \bar{u}(z)}{\partial z}$ in this case of a 1D turbulent boundary layer. The turbulent viscosity is calculated in a similar fashion to the standard *k-ε* model

$$\nu_\mathrm{t}(z) = C_{\mu\_\mathrm{rke}}(z)\frac{k(z)^2}{\varepsilon(z)} \tag{10}$$

whereas C_{μ_rke} is no longer a constant, as was the case with C_{μ_ske} in the standard *k-ε* turbulence model. Instead, C_{μ_rke} is determined as follows

$$C_{\mu\_\mathrm{rke}}(z) = \frac{1}{A_{0\_\mathrm{rke}} + A_\mathrm{s}(z)U^*(z)\frac{k(z)}{\varepsilon(z)}} \tag{11}$$

where

$$U^*(z) = \sqrt{S_{ij}(z)S_{ij}(z) + \tilde{\Omega}_{ij}(z)\tilde{\Omega}_{ij}(z)} \tag{12}$$

$$\tilde{\Omega}(z)=\frac{1}{2}\left(\frac{\partial u_i}{\partial x_j}-\frac{\partial u_j}{\partial x_i}\right) \tag{13}$$

which simplifies to

$$\tilde{\Omega}(z)=\frac{1}{2}\frac{\partial \bar{u}(z)}{\partial z} \tag{14}$$

The model has five coefficients, and their standard values are: $A_{0\_\mathrm{rke}}=4.04$, $\sigma_{k\_\mathrm{rke}}=1.0$, $\sigma_{\varepsilon\_\mathrm{rke}}=1.2$, $C_{2\_\mathrm{rke}}=1.9$, and $C_{1\_\mathrm{rke}}=\max\{0.43,\frac{\eta(z)}{\eta(z)+5}\}$, where $\eta(z)$ is the ratio between the magnitude of the strain tensor, turbulent kinetic energy and the turbulence dissipation, mathematically expressed as $\eta(z)=\frac{S(z)k(z)}{\varepsilon(z)}$. Furthermore, the function $A_S(z)$ required for the calculation of $C_{\mu\_\mathrm{rke}}(z)$ is a function of the strain tensor and it is obtained from the following set of equations

$$A_S(z)=\sqrt{6}\cos\varphi(z) \tag{15}$$

$$\varphi(z)=\frac{1}{3}\arccos(\sqrt{6}W(z)) \tag{16}$$

$$W(z)=\frac{S_{ij}(z)S_{jk}(z)S_{ki}(z)}{\tilde{S}^3(z)} \tag{17}$$

$$\tilde{S}(z)=\sqrt{S_{ij}(z)S_{ij}(z)} \tag{18}$$

In addition, Shih *et al*. (1995) have shown that in the log-law boundary layer the following equation shall be satisfied in order to minimize the modeling error

$$\sigma_{\varepsilon\_\mathrm{rke}}=\frac{\kappa^2}{C_{2\_\mathrm{rke}}\sqrt{C_{\mu\_\mathrm{rke}}(z)}-C_{1\_\mathrm{rke}}} \tag{19}$$

While the standard coefficients for this turbulence model are calibrated for the standard channel flow where $C_{\mu\_\mathrm{rke}}=0.09$, the measurements presented in the previous section show that the required value is $C_{\mu\_\mathrm{rke}}=0.044$. Moreover, in case of the atmospheric boundary layer flow it is possible to show that the function $\eta(z)$ becomes $\eta(z)=\sqrt{1/C_{\mu\_\mathrm{rke}}(z)}$.

The coefficient A_{0_rke} calculated from Eq. (11) yields $A_{0\_\mathrm{rke}}=12.6$. By calculating the coefficient C_{1_rke} from the current value of C_{μ_rke} and by using it in Eq. (19), it can be shown that $\sigma_{\varepsilon\_\mathrm{rke}}$ becomes negative. By comparing the constants C_{1_rke} and C_{1_ske} it reveals that the value 0.43 in the function for determining C_{1_rke} is obtained by multiplying the

C_{1_ske} of the standard *k*-ε model with the square root of the standard value for C_{μ_rke}. Furthermore, it is also possible to show that the term $\frac{\eta(z)}{\eta(z)+5}$ is not dominant in case of the 1D boundary layer flow, and the value 5 is chosen to make this term 7% smaller than the left part of the equation. This has motivated the modification of the coefficient C_{1_rke} into the form which is valid even when the coefficients are altered

$$C_{1\_rke} = \max\{\sqrt{C_{\mu\_rke}(z)}\, C_{1\_ske}, \frac{\eta(z)}{\eta(z)+K(z)}\} \tag{20}$$

and *K*(*z*) is calculated as follows

$$K(z) = 1.075\frac{1-\sqrt{C_{\mu\_rke}(z)}\, C_{1\_rke}}{\sqrt{C_{\mu\_rke}(z)}\, C_{1\_rke}} \tag{21}$$

Finally, the coefficients used for all calculations using this model are $A_{0\_rke} = 12.06$, $C_{2\_rke} = 1.9$, $\sigma_{k\_rke} = 1.0$ and $\sigma_{\varepsilon\_rke} = 1.7$.

3.3 The RNG k-ε turbulence model

The RNG *k*-ε model developed by Yakhot and Orszag (1986) is a two-equation turbulence model that solves an equation for turbulent kinetic energy $k(z)$ and an equation for turbulence dissipation, $\varepsilon(z)$. It is designed to improve prediction of turbulent kinetic energy in flow stagnation zones. The equation for the turbulent kinetic energy is given in Eq. (3) and the equation for the turbulence dissipation is as follows

$$\frac{\partial}{\partial z}\left[\frac{\nu_t(z)}{\sigma_{\varepsilon\_rng}}\frac{\partial\varepsilon(z)}{\partial z}\right] + C_{1\_rng}(z)\frac{P(z)}{k(z)}\cdot\varepsilon(z) - C_{2\_rng}\frac{\varepsilon^2(z)}{k(z)} = 0 \tag{22}$$

The turbulent viscosity is calculated in the same fashion as for the standard *k*-ε turbulence model, as given in Eq. (5). The main difference of this model from the standard *k*-ε model is in $C_{1\_rng}(z)$, which is no longer a constant but is calculated based on the local flow parameters as follows

$$C_{1\_rng}(z) = C_{1\_rng} - \frac{\eta(z)(1-\eta(z)/\eta_0)}{1+\beta_{rng}\eta^3(z)} \tag{23}$$

$\eta(z)$ has the same form as for the realizable *k*-ε model, which for 1D boundary layer flow simplifies to $\eta(z) = \sqrt{1/C_\mu(z)}$.

This turbulence model has seven coefficients i.e., C_{μ_rng}, σ_{k_rng}, $\sigma_{\varepsilon\_\mathrm{rng}}$, C_{1_rng}, C_{2_rng}, η_{0_rng} and β_{rng} with their standard values $C_{\mu\_\mathrm{rng}}=0.0845$, $\sigma_{k\_\mathrm{rng}}=0.71942$, $\sigma_{\varepsilon\_\mathrm{rng}}=0.71942$, $C_{1\_\mathrm{rng}}=1.42$, $C_{2\_\mathrm{rng}}=1.68$, $\eta_{0\_\mathrm{rng}}=4.38$ and $\beta_{\mathrm{rng}}=0.012$.

The experimental results reported in the previous section indicate that the value of the coefficient C_{μ_rng} needs to be reduced to $C_{\mu\_\mathrm{rng}}=0.044$ in order to correctly calculate the ratio between the turbulent kinetic energy and the dominant component of the turbulent shear stress. In order to achieve the same C_{2_rng} coefficient as for C_{2_ske} in the *k*-ε model, the value of η_0 increases to $\eta_0=6.2$. Finally, the value of $\sigma_{\varepsilon\_\mathrm{rng}}$ is calculated from Eq. (8) and has the value $\sigma_{\varepsilon\_\mathrm{rng}}=1.08$. Therefore, the values of the coefficients used for all calculations using this turbulence model are $C_{\mu\_\mathrm{rng}}=0.044$, $C_{1\_\mathrm{rng}}=1.42$, $C_{2\_\mathrm{rng}}=1.68$, $\sigma_{k\_\mathrm{rng}}=0.71942$, $\sigma_{\varepsilon\_\mathrm{rng}}=1.08$, $\eta_{0\_\mathrm{rng}}=6.2$, and $\beta_{\mathrm{rng}}=0.012$.

3.4 The k-ω turbulence model

The *k*-ω turbulence model developed by Wilcox (1988) is a two-equation turbulence model, which solves an equation for turbulent kinetic energy $k(z)$ and an equation for specific turbulence dissipation $\omega(z)$. The equation for the turbulent kinetic energy is

$$\frac{\partial}{\partial z}\left[\sigma^{*}_{k\omega}\nu_{\mathrm{t}}(z)\frac{\partial k(z)}{\partial z}\right]+P(z)-\beta^{*}_{k\omega}\omega(z)k(z)=0 \tag{24}$$

and the equation for the specific turbulence dissipation $\omega(z) = \varepsilon(z)/k(z)$ has the form

$$\frac{\partial}{\partial z}\left[\sigma_{k\omega}\nu_{\mathrm{t}}(z)\frac{\partial \omega(z)}{\partial z}\right]+\gamma_{k\omega}\frac{P(z)\omega(z)}{k(z)}-\beta_{k\omega}\omega^{2}(z)=0 \tag{25}$$

The turbulent viscosity ν_{t} is calculated as a ratio between the turbulent kinetic energy $k(z)$ and the specific turbulence dissipation $\omega(z)$

$$\nu_{\mathrm{t}}(z)=\gamma^{*}_{k\omega}\frac{k(z)}{\omega(z)} \tag{26}$$

This turbulence model has six constants $\beta_{k\omega}$, $\beta^{*}_{k\omega}$, $\gamma_{k\omega}$, $\gamma^{*}_{k\omega}$, $\sigma_{k\omega}$, and $\sigma^{*}_{k\omega}$ with the standard values $\beta_{k\omega}=3/40$, $\beta^{*}_{k\omega}=9/100$, $\gamma_{k\omega}=5/9$, $\gamma^{*}_{k\omega}=1$, $\sigma_{k\omega}=1/2$ and $\sigma^{*}_{k\omega}=1/2$ (Wilcox 1988). In the wind-tunnel experiments used to validate computations carried out in this study, the measured ratio between the dominant component of the shear stress and the turbulent kinetic energy is 4.76 which implies that $\beta^{*}_{k\omega}=0.044$. In addition, Wilcox (1988) indicated the ratio $\beta^{*}_{k\omega}/\beta_{k\omega}=6/5$ necessary to correctly simulate the effect of the decaying turbulence that

gives $\beta_{k\omega} = 0.0367$. The last remaining coefficient which requires special attention is $\gamma_{k\omega}$. It is obtained from the expression valid in the log-law layer

$$\gamma_{k\omega} = \frac{\beta_{k\omega}}{\beta^*_{k\omega}} - \frac{\sigma_{k\omega}\kappa^2}{\sqrt{\beta^*_{k\omega}}} \tag{27}$$

which gives $\gamma_{k\omega} = 0.43$. All calculations in this study using the *k*-ω turbulence model are performed with the same set of coefficients which are $\beta_{k\omega} = 0.037$, $\beta^*_{k\omega} = 0.044$, $\gamma_{k\omega} = 0.43$, $\gamma^*_{k\omega} = 1$, $\sigma_{k\omega} = 1/2$ and $\sigma^*_{k\omega} = 1/2$. Please note that the coefficients $\sigma_{k\omega} = 1/2$ and $\sigma^*_{k\omega} = 1/2$ were not modified due to the inexistence of any analytical expression. Wilcox (1988) argues that those two coefficients are evaluated empirically and they represent the minimum error for all flows used for calibration.

4. Numerical setup

Computational simulations were carried out by using OpenFOAM, an open source CFD toolbox. For each terrain type the computational domain was a 2D cut through the symmetry plane of the wind-tunnel test section, whereas the results were sampled at 21.9 m downwind from the inlet. Calculations were performed and presented at the wind-tunnel scale. The geometry of the computational domain is presented in Fig. 2.

The slope of the ceiling in the computational domain is set to comply with respective values in the ABL wind-tunnel simulations for different terrain types. The value of pressure is set to be constant with height at inlet and outlet boundaries. The streamwise gradient of $u(z)$, $k(z)$, $\varepsilon(z)$, $\omega(z)$ fields is set to zero at both inlet and outlet boundaries. In addition, those boundary conditions do not guarantee homogeneity of the flow conditions in the longitudinal direction as the height of the upper wall changes throughout the domain. However, the focus of this study was to obtain agreement with the experimental results at the sampling position for the tested turbulence models, rather than to achieve homogeneous flow conditions along the computational domain. The similar approach is commonly used in the wind tunnels, where different types of experimental hardware are employed to simulate the ABL, and it is required to have a sufficient fetch to allow for developing of the flow and turbulence. In addition, the height of the wind-tunnel test section changes in longitudinal direction in order to approach zero-pressure gradient conditions in the streamwise direction.

The walls of the geometry are treated as rough walls, where the following wall-function was implemented in the code

$$\frac{\tau_w}{\rho} = \frac{\bar{u}(z_C)u_\tau\kappa}{\ln\frac{z_C + z_0}{z_0}} \tag{28}$$

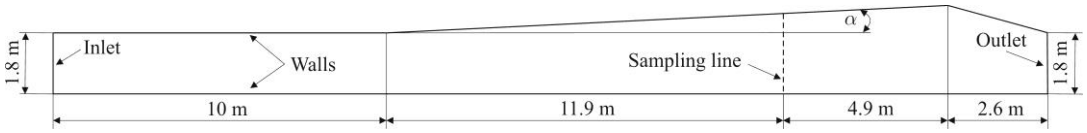

Fig. 2 Geometry and dimensions of the computational domain as reported in Juretić and Kozmar (2013)

where z_C is the distance of the centre of the near-wall cell from the wall. The value of u_τ is calculated as $u_\tau = \sqrt[4]{C_\mu}\sqrt{\bar{k}(z_C)}$, where the coefficient C_μ was calculated for a particular turbulence model as respectively defined in a previous section. The gradient of the turbulent kinetic energy $k(z)$ is set to zero in the direction normal to the wall which is a common procedure for the log-law region. The turbulence production $P(z)$ in the wall function is set to $P_C = \tau_w \nabla \bar{u}(z_C)$, as it is commonly used in the OpenFOAM code. The values of z_0 at the bottom wall were calculated to force the code to re-create the same velocity and shear stress at the wall as the measured values by using the equation $z_0 = z_C/(e^D - 1)$, where z_C is the distance of the center in the near-wall cell from the wall, D is $\bar{u}(z_C)\kappa/u_\tau$, and $\bar{u}(z_c)$ is the measured average velocity at the given distance. The value of the turbulence dissipation in the near-wall cell is set to

$$\varepsilon_C = \frac{{u_\tau}^3}{\kappa(z_C + z_0)} \tag{29}$$

The value of the specific turbulence dissipation in the near-wall cells is set to

$$\omega_C = \frac{u_\tau}{\kappa(z_C + z_0)} \tag{30}$$

The coupled system is solved by using the second-order accurate discretization procedure (Jasak 1996 and Juretić 2004). The equations are coupled by using the SIMPLE (Semi-Implicit procedure for Pressure-Linked Equations) algorithm (Patankar and Spalding 1972). The equations are solved until the scaled residual is reduced below 10^{-7} such that the solution error of the system of algebraic equations is negligible compared to the discretization error, as well as the turbulence model error. The convection terms are approximated using Gamma differencing scheme (Jasak 1996, Jasak *et al*. 1999) for all convection terms. In order to check and control discretization accuracy, grid sensitivity was investigated, and the reported results do not differ from the results on a coarser mesh by more than 1%.

5. Computational results

In this section, the results obtained in computational simulations are presented and compared against the wind-tunnel results. The parameters which are compared are mean velocity, turbulent kinetic energy, Reynolds shear stress, as they are considered to be the key factors influencing local wind environment with likely effects on structures.

Table 2 shows the angles of the top wall and the aerodynamic surface roughness length z_0 applied at the bottom and the upper wall for all terrain types.

The applied aerodynamic surface roughness length z_0 at the bottom wall has approximately double the values recorded in the wind tunnel, while the first cell above the wall has a center at the same distance from the wall as z_0. The values in Table 2 were calculated using the expression for z_0 addressed above and the measured Reynolds shear stress close to the bottom wall.

In this section, the results will be presented for all four turbulence models and three different terrain types investigated. Computational results will be reported in the range of available experimental values, i.e., from 0.1 m up to 1 m height. The mean velocity profiles calculated using the four turbulence models for three terrains are presented in Fig. 3. The height *z* from the surface is given at the wind-tunnel scale, whereas both experimental and computational results for mean velocity are nondimensionalized using the experimental results for $\bar{u}_{\mathrm{ref}}$ recorded at *z* = 0.202 m reported in Table 1.

For all terrain types, the three *k*-ε models yield similar results that is expected because they can all be simplified to the same form in case of the 1D ABL flow. On the other hand, the *k*-ω profiles indicate slightly different trend in comparison to the *k*-ε models. In particular, while the *k*-ω model compares better to the experimental results for rural and suburban type terrain, in the urban configuration the *k*-ω model under-predicts the measured velocity, and it is consistently more diffusive for all types of terrains than the *k*-ε counterparts. This is possibly due to the $\sigma_{k\omega}$ and $\sigma^*_{k\omega}$ coefficients, which are not modified even though all other coefficients were changed. Furthermore, it is also not completely clear how the modification of those coefficients could potentially affect the performance of this model for complex flows. The profiles for all turbulence models are within ±10% threshold with respect to the experimental data.

Table 2 Aerodynamic surface roughness length z_0 at the bottom and top walls of the computational domain, and the angle of the top wall applied in the computational domain (Juretić and Kozmar 2013)

Case	z_0 at the bottom wall, m	z_0 at the top wall, m	α, ^{0}
Rural	$1.70 \cdot 10^{-3}$	$1 \cdot 10^{-9}$	0.2
Suburban	$4.00 \cdot 10^{-3}$	$1 \cdot 10^{-5}$	0.3
Urban	$1.55 \cdot 10^{-2}$	$5 \cdot 10^{-4}$	0.8

Table 3 The model coefficients used for the ABL simulations with all four turbulence models

Turbulence model	Coefficients
Standard *k*-ε	$C_{\mu\_ske} = 0.044$, $C_{1\_ske} = 1.44$, $C_{2\_ske} = 1.92$, $\sigma_{k\_ske} = 1$, $\sigma_{\varepsilon\_ske} = 1.67$
Realizable *k*-ε	$A_{0\_rke} = 12.06$, $C_{2\_rke} = 1.9$, $\sigma_{k\_rke} = 1.0$, $\sigma_{\varepsilon\_rke} = 1.7$
RNG *k*-ε	$C_{\mu\_rng} = 0.044$, $C_{1\_rng} = 1.42$, $C_{2\_rng} = 1.68$, $\sigma_{k\_rng} = 0.71942$, $\sigma_{\varepsilon\_rng} = 1.08$, $\eta_{0\_rng} = 6.2$, $\beta_{rng} = 0.012$
k-ω	$\beta_{k\omega} = 0.037$, $\beta^*_{k\omega} = 0.044$, $\gamma_{k\omega} = 0.43$, $\gamma^*_{k\omega} = 1$, $\sigma_{k\omega} = 1/2$, $\sigma^*_{k\omega} = 1/2$

The model coefficients used for the ABL simulations with all four turbulence models are provided in Table 3.

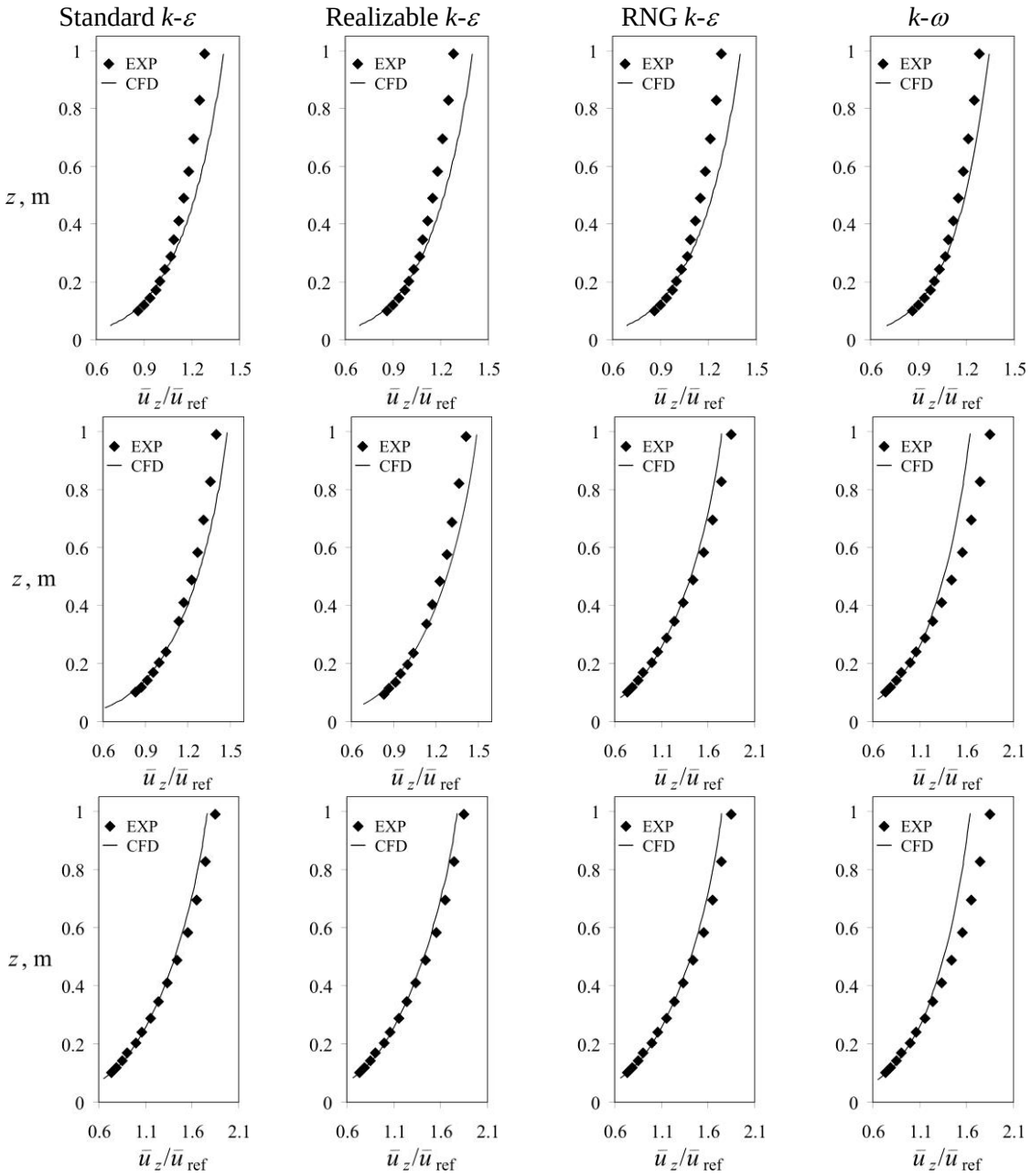

Fig. 3 Comparison of the mean velocity profiles in wind-tunnel experiments (EXP) and computational simulations (CFD); results for the standard k-ε (first column), realizable k-ε (second column), RNG k-ε (third column), k-ω (fourth column) turbulence models are presented for rural (first row), suburban (second row), and urban (third row) type terrains

The turbulent kinetic energy profiles calculated using the four turbulence models for three terrains are presented in Fig. 4, where height z from the surface is given at the wind-tunnel scale.

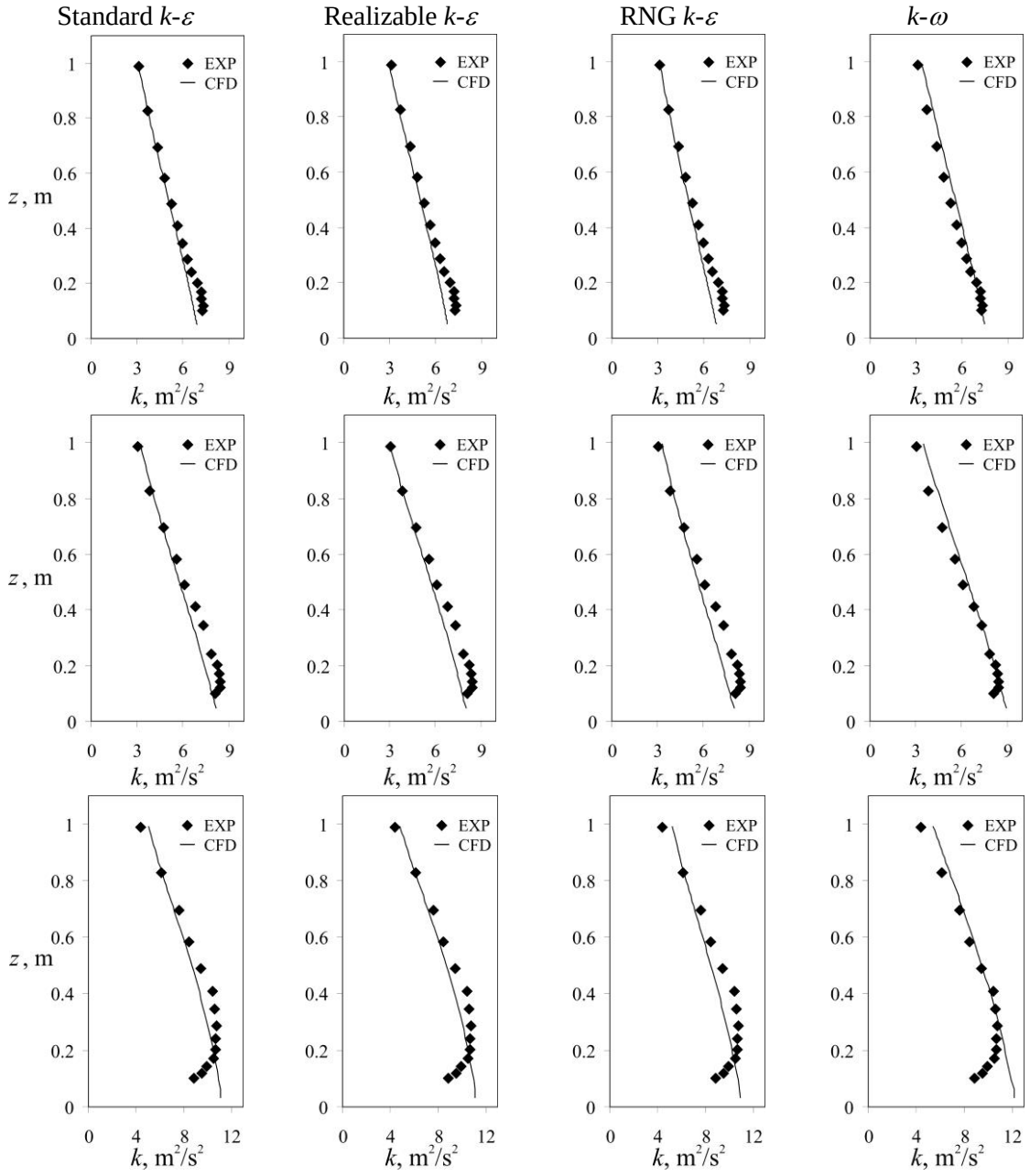

Fig. 4 Comparison of the turbulent kinetic energy profiles in wind-tunnel experiments (EXP) and computational simulations (CFD); results for the standard k-ε (first column), realizable k-ε (second column), RNG k-ε (third column), k-ω (fourth column) turbulence models are presented for rural (first row), suburban (second row), and urban (third row) type terrains

In general, the computational results agree well with the experiments, particularly for the rural type terrain, whereas, for all terrain types, the differences between the computational and experimental results are larger close to the bottom surface of the computational domain. In particular, with increased urbanization at the ground surface, the curvature of the turbulent kinetic energy profile becomes more exhibited in the lower ABL experimental simulation, and the computational models are not fully capable of following this trend. In addition, the current boundary conditions require the zero-gradient boundary condition normal to the wall, commonly adopted by other modelers, which prevents the turbulent kinetic energy to decrease to zero at the surface. In addition, for the rural and suburban terrains there exists a region with a steep decrease in the lower ABL wind-tunnel profiles that cannot be captured by using the k-ε turbulence models due to a lack of source terms which enforce this behavior. Hence, it can generally be observed that for the turbulent kinetic energy profiles the k-ω performs slightly better than the k-ε turbulence models. In most parts of the flow, the computational results for all turbulence models are within ±10% threshold with respect to the experimental data.

The Reynolds shear stress profiles calculated using the four turbulence models for three terrains are presented in Fig. 5. The height z from the surface is given at the wind-tunnel scale, whereas both experimental and computational results are nondimensionalized using the experimental results for u_τ reported in Table 1.

The reported results indicate that the calculated and the measured Reynolds shear stress profiles are within the 10% threshold for all turbulence models and terrain types. The profiles for the k-ε models all look similar. In particular, for the rural and suburban terrain type, the discrepancy between the computational and experimental data is larger near the wall due to a lack of source terms that would allow for a rapid increase/decrease of the turbulence in the fluid. For the urban terrain type, this difference is larger at mid heights of the ABL simulation around z = 0.4 m. The differences between the experimental data and the profiles calculated by using the k-ω turbulence model are consistently distributed over the height and they are generally smaller than that is the case with k-ε models, particularly close to the surface.

The turbulent kinetic energy to Reynolds shear stress ratio calculated using the four turbulence models for three terrains is presented in Fig. 6, whereas the height z from the surface is given at the wind-tunnel scale.

Similarly as for the turbulent kinetic energy and Reynolds shear stress profiles, the computational results for all turbulence models agree well in the upper parts of the ABL simulations, while they are not able to fully capture the profile curvature close to surface in the urban configuration. This is due to the zero-gradient boundary condition imposed at the bottom wall of the computational domain that is not in agreement with full-scale conditions and particularly exhibited for the urban type terrain.

6. Conclusions

This study has attempted to improve the currently-existing methodology for computational modeling of the neutrally stratified atmospheric boundary layer, by using various two-equation turbulence models and the steady Reynolds-Averaged-Navier-Stokes equations. This approach accounts for a decrease in turbulence parameters with height without a need to add additional terms to the turbulence models. Four different two-equation turbulence models (standard k-ε,

realizable k-ε, RNG k-ε, k-ω) were tested using this approach in a computational domain that mimics wind-tunnel experiments for flow and turbulence developing above rural, suburban, and urban type terrains.

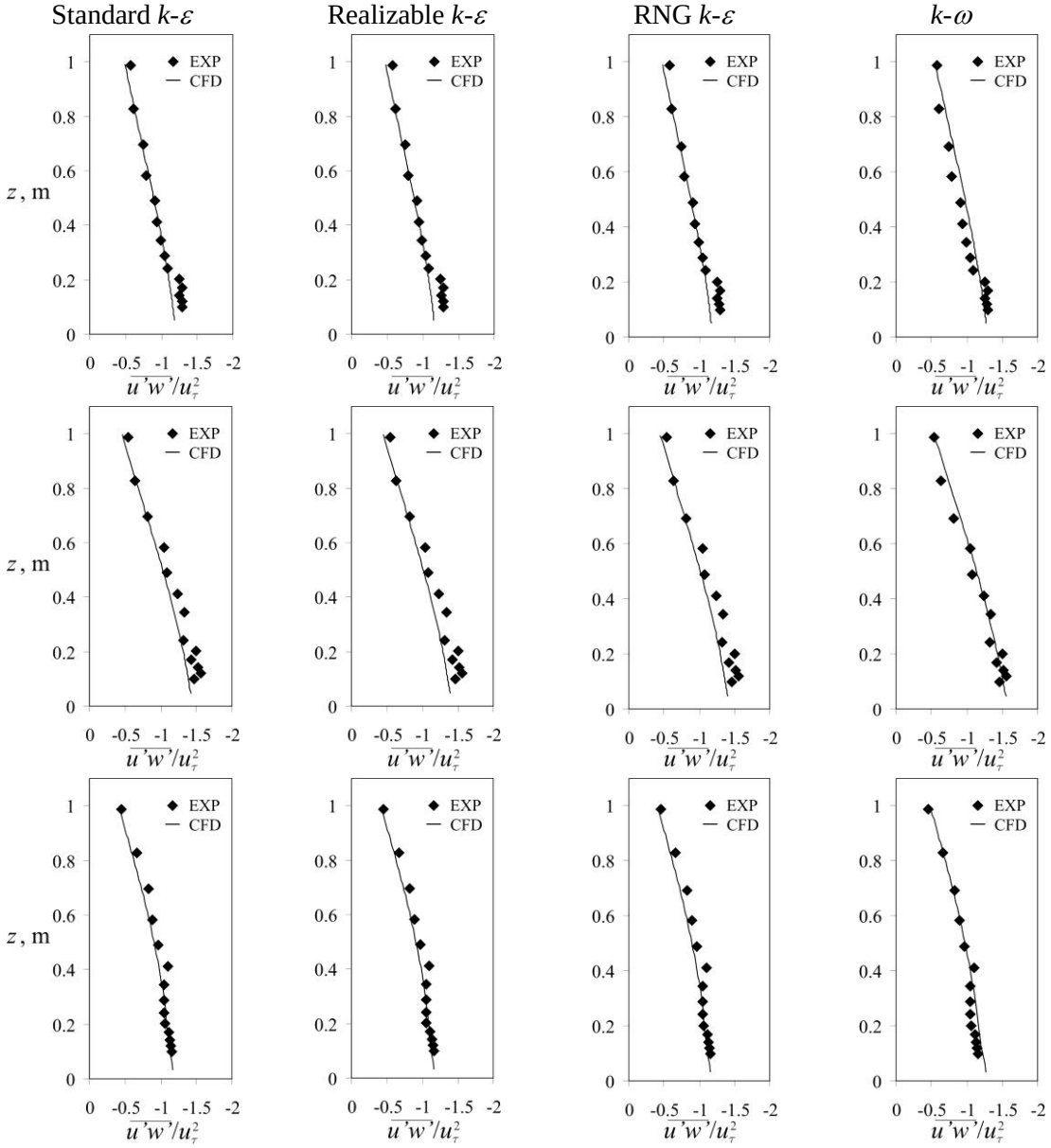

Fig. 5 Comparison of the Reynolds shear stress profiles in wind-tunnel experiments (EXP) and computational simulations (CFD); results for the standard k-ε (first column), realizable k-ε (second column), RNG k-ε (third column), k-ω (fourth column) turbulence models are presented for rural (first row), suburban (second row), and urban (third row) type terrains

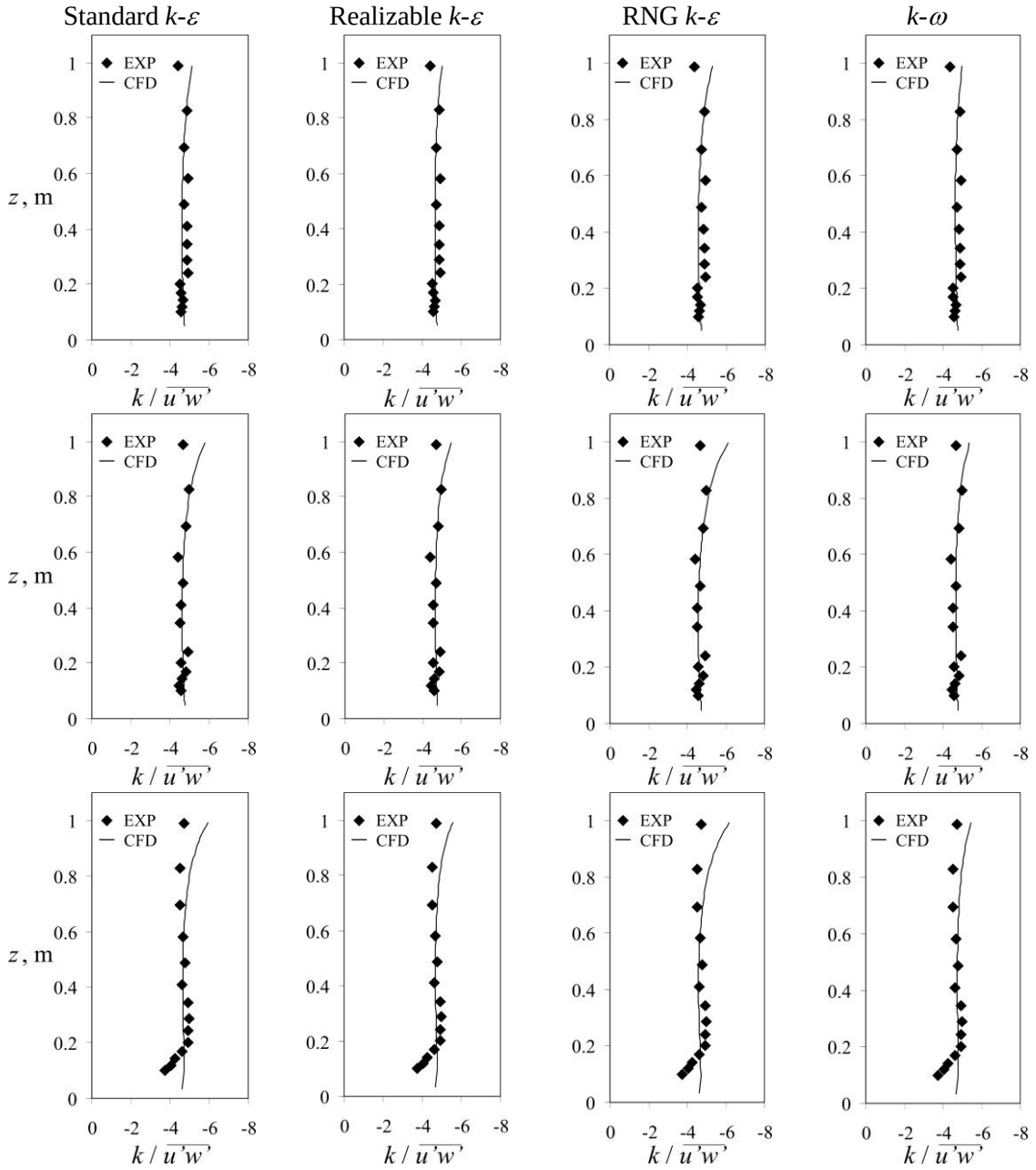

Fig. 6 Comparison of the turbulent kinetic energy to Reynolds shear stress ratio in wind-tunnel experiments (EXP) and computational simulations (CFD); results for the standard k-ε (first column), realizable k-ε (second column), RNG k-ε (third column), k-ω (fourth column) turbulence models are presented for rural (first row), suburban (second row), and urban (third row) type terrains

In general, the computational results agree very well with experimental results. In particular, the difference between the calculated and measured mean velocity, turbulent kinetic energy and Reynolds shear stress profiles is less than ±10% in most parts of the computational domain. The results obtained indicate that the *k*-ε models produce consistent results. The *k*-ω model performs better in terms of the predicted Reynolds shear stress and the turbulent kinetic energy, and it is more diffusive in terms of the mean velocity profiles when compared to the *k*-ε models. This is attributed to the $\sigma_{k\omega}$ and $\sigma^{*}_{k\omega}$ coefficients which were not modified due to a lack of explicit expression, and their standard values proved to minimize the error for all flows used for calibration. Future work is needed to address boundary conditions at the walls, which are currently not consistent with the measured results in the limit of the very fine mesh near the wall. In addition, it is believed that the *k*-ω model can be further improved by analyzing the influence of the $\sigma_{k\omega}$ and $\sigma^{*}_{k\omega}$ coefficients in the 1D boundary layer flow, as well as by performing the computations all the way down to the bottom wall instead of using the wall functions. More work is needed in order to further validate this methodology with respect to flow around buildings including flow separation, reattachment and other aerodynamic phenomena.

Acknowledgements

The second author acknowledges support of the Croatian Ministry of Science and Technology, the German Academic Exchange Service (DAAD), the Croatian Academy of Sciences and Arts (HAZU), and the Institute of Aerodynamics and Fluid Mechanics, Faculty of Mechanical Engineering, Technische Universität München (TUM) with respect to wind-tunnel experiments.

References

Blocken, B., Stathopoulos, T. and Carmeliet, J. (2007a), "CFD simulation of the atmospheric boundary layer: wall function problems", *Atmos. Environ.*, **41**(2), 238-252.

Blocken, B., Carmeliet, J. and Stathopoulos, T. (2007b), "CFD evaluation of wind speed conditions in passages between parallel buildings - effect of wall-function roughness modifications for the atmospheric boundary layer flow", *J. Wind Eng. Ind. Aerod*., **95**(9-11), 941-962.

Boussinesq, J. (1877), "Essai sur la theorie des eaux courantes", Memoires presentes par divers savants al'Academie des Sciences **XXIII**, 1-680.

Counihan, J. (1969a), "A method of simulating a neutral atmospheric boundary layer in a wind tunnel", AGARD Conference Proceedings 43.

Counihan, J. (1969b), "An improved method of simulating an atmospheric boundary layer in a wind tunnel", *Atmos. Environ.*, **3**, 197-214.

Counihan, J. (1973), "Simulation of an adiabatic urban boundary layer in a wind tunnel", *Atmos. Environ.*, **7**(7), 673-689.

Duynkerke, P.G. (1988), "Application of the E-epsilon turbulence closure-model to the neutral and stable atmospheric Boundary Layer", *J. Atmos. Sci.*, **45**(5), 865-880.

ESDU 74031 (1974), "Characteristics of atmospheric turbulence near the ground. Part II: single point data for strong winds (neutral atmosphere)", Engineering Sciences Data Unit 74031.

Franke, J., Hellsten, A., Schlünzen, H. and Carissimo, B.E. (2007), "Best practice guideline for the CFD simulation of flows in the urban environment", Cost action 732: quality assurance and improvement of microscale meteorological models.

Garratt, J.R. (1992), *The atmospheric boundary layer*, Cambridge University Press, New York, NY, USA.
Gorlé, C., van Beeck, J., Rambaud, P. and Van Tendeloo, G. (2009), "CFD modelling of small particle dispersion: The influence of the turbulence kinetic energy in the atmospheric boundary layer", *Atmos. Environ.*, **43**(3), 673-68.
Hargreaves, D.M. and Wright, N.G. (2007), "On the use of the *k-ε* model in commercial CFD software to model the neutral atmospheric boundary layer", *J. Wind Eng. Ind. Aerod.*, **95**(5), 355-369.
Holmes, J.D. (2007), *Wind loading of structures*, 2nd Ed., Taylor & Francis, London, UK.
Hu, P., Li, Y.L., Cai, C.S., Liao, H.L. and Xu, G.J. (2013), "Numerical simulation of the neutral equilibrium atmospheric boundary layer using the SST k-omega turbulence model", *Wind Struct.*, **17**(1), 87-105.
Jasak, H. (1996), *Error analysis and estimation in the finite volume method with application to fluid flows*, Ph.D. Thesis, Imperial College, University of London, London, UK.
Jasak, H., Weller, H. and Gosman, A. (1999), "High resolution NVD differencing scheme for arbitrarily unstructured meshes", *Int. J. Numer. Meth. Fl.*, **31**, 431-449.
Jones, W.P. and Launder B.E. (1972), "The prediction of laminarization with a two-equation model of turbulence", *Int. J. Heat Mass Trans.*, **15**(2), 301-314.
Juretić, F. (2004), *Error analysis in finite volume CFD*, Ph.D. Thesis, Imperial College, University of London, London, UK.
Juretić, F. and Kozmar, H. (2013), "Computational modeling of the neutrally stratified atmospheric boundary layer flow using the standard *k-ε* turbulence model", *J. Wind Eng. Ind. Aerod.*, **115**, 112-120.
Kozmar, H. (2008), "Influence of spacing between buildings on wind characteristics above rural and suburban areas", *Wind Struct.*, **11**(5), 413-426.
Kozmar, H. (2010), "Scale effects in wind tunnel modeling of an urban atmospheric boundary layer", *Theor. Appl. Climatol.*, **100**(1-2), 153-162.
Kozmar, H. (2011a), "Truncated vortex generators for part-depth wind-tunnel simulations of the atmospheric boundary layer flow", *J. Wind Eng. Ind. Aerod.*, **99**(2-3), 130-136.
Kozmar, H. (2011b) "Characteristics of natural wind simulations in the TUM boundary layer wind tunnel", *Theor. Appl. Climatol.*, **106**(1-2), 95-104.
Kozmar, H. (2011c), "Wind-tunnel simulations of the suburban ABL and comparison with international standards", *Wind Struct.*, **14**(1), 15-34.
Kozmar, H. (2012a), "Improved experimental simulation of wind characteristics around tall buildings", *J. Aerospace Eng.*, **25**(4), 670-679.
Kozmar, H. (2012b), "Physical modeling of complex airflows developing above rural terrains", *Environ. Fluid Mech.*, **12**(3), 209-225.
O'Sullivan, J.P., Archer, R.A. and Flay, R.G.J. (2011), "Consistent boundary conditions for flows within the atmospheric boundary layer", *J. Wind Eng. Ind. Aerod*., **99**(1), 65-77.
Parente, A., Gorlé, C., van Beeck, J. and Benocci, C. (2011a), "Improved *k-ε* model and wall function formulation for the RANS simulation of ABL flows", *J. Wind Eng. Ind. Aerod.*, **99**(4), 267-278.
Parente, A., Gorlé, C., van Beeck, J. and Benocci, C. (2011b), "A comprehensive modelling approach for the neutral atmospheric boundary layer: Consistent inflow conditions, wall function and turbulence model", *Bound. - Lay. Meteorol.*, **140**, 411-428.
Patankar, S.V. and Spalding, D.B. (1972), "A calculation procedure for heat, mass and momentum transfer in three-dimensional parabolic flows", *Int. J. Heat Mass Trans.*, **15**(10), 1787-1806.
Pope, S.B. (2000), *Turbulent Flows*, Cambridge University Press, Cambridge, UK.
Revuz, J., Hargreaves, D.M. and Owen J.S. (2012), "On the domain size for the steady-state CFD modelling of a tall building", *Wind Struct.*, **15**(4), 313-329.
Richards, P.J. and Hoxey, R.P. (1993), "Appropriate boundary conditions for computational wind engineering models using the *k-ε* turbulence model", *J. Wind Eng. Ind. Aerod.*, **46-47**, 145-153.
Riddle, A., Carruthers, D., Sharpe, A., McHugh, C. and Stocker, J. (2004), "Comparisons between FLUENT and ADMS for atmospheric dispersion modeling", *Atmos. Environ.*, **38**(**7**), 1029-1038.

Shih, T.H., Liou, W.W., Shabbir, A., Yang, Z. and Zhu, J. (1995), "A new k-ϵ eddy viscosity model for high Reynolds number turbulent flows", *Comput. Fluids*, **24**(3), 227-238.

Wilcox, D.C. (1988), "Reassessment of the scale-determining equation for advanced turbulence models", *AIAA J.*, **26**(11), 1299-1310.

Yakhot, V. and Orszag, S.A. (1986), "Renormalization group analysis of turbulence, 1. Basic Theory", *J. Sci. Comput.*, **1**, 3-51.

Yang, Y., Gu, M., Chen, S. and Jin, X. (2009), "New inflow boundary conditions for modelling the neutral equilibrium atmospheric boundary layer in computational wind engineering", *J. Wind Eng. Ind. Aerod.*, **97**(2), 88-95.

Zhang, J., Yang, Q.S. and Li, Q.S. (2013), "Developments and applications of a modified wall function for boundary layer flow simulations", *Wind Struct.*, **17**(4), 361-377.

JH

Nomenclature

$k(z)$	Turbulent kinetic energy
$\bar{p}(z)$	Kinematic air pressure
$u(z), v(z), w(z)$	Instantaneous velocity components in the *x*-, *y*-, *z*-direction, respectively
$\bar{u}(z), \bar{v}(z), \bar{w}(z)$	Mean velocity components in the *x*-, *y*-, *z*-direction, respectively
u', v', w'	Fluctuating velocity components in the *x*-, *y*-, *z*-direction, respectively
$\overline{u'w'}(z)$	Reynolds shear stress
$\bar{u}_{\mathrm{ref}}$	Mean reference velocity at the reference height z_{ref}
u_τ	Friction velocity
x	Distance in the main flow direction
y	Spanwise distance from the test section centre plane
z	Vertical distance from the wind-tunnel floor and the bottom of the computational domain
z_{C}	Distance of the center in the near-wall cell from the wall
z_{ref}	Reference height
z_0	Aerodynamic surface roughness length
$A_{\mathrm{S}}(z)$	Function of the strain tensor
C_{μ_ske}, σ_{k_ske}, $\sigma_{\varepsilon\_\mathrm{ske}}$, C_{1_ske}, C_{2_ske}	Constants of the standard *k*-ε turbulence model
A_{0_rke}, σ_{k_rke}, $\sigma_{\varepsilon\_\mathrm{rke}}$, C_{2_rke}, C_{1_rke}	Constants of the realizable *k*-ε turbulence model
$\omega_k(z)$, $\eta(z)$, $\varphi(z)$, $W(z)$, $K(z)$, $U^*(z)$	Parameters in the realizable *k*-ε turbulence model
C_{μ_rng}, σ_{k_rng}, $\sigma_{\varepsilon\_\mathrm{rng}}$, C_{1_rng}, C_{2_rng}, η_{0_rng}, β_{rng}	Constants of the RNG *k*-ε turbulence model
$\beta_{k\omega}$, $\beta^*_{k\omega}$, $\gamma_{k\omega}$, $\gamma^*_{k\omega}$, $\sigma_{k\omega}$, $\sigma^*_{k\omega}$	Constants of the *k*-ω turbulence model
D	Non-dimensional parameter
I_u, I_v, I_w	Turbulence intensity in the *x*-, *y*-, *z*-direction, respectively
$P(z)$	Production term

$S(z)$	Magnitude of the strain tensor
P_C	Turbulence production P in the near-wall cell
α	Power-law exponent
$\varepsilon(z)$	Turbulence dissipation
ε_C	Turbulence dissipation ε in the near-wall cell
κ	Von Kármán constant
μ	Dynamic laminar viscosity
ν_t	Laminar kinematic viscosity
$\nu_t(z)$	Kinematic turbulent (eddy) viscosity
ρ	Fluid density
τ_w	Shear stress at the wall
ω	Specific turbulence dissipation
ω_C	Specific turbulence dissipation in the near-wall cell
$\Omega(z)$	Rate-of-rotation tensor
$\overline{\Omega}(z)$	Average rate-of-rotation tensor